GRADIENT-BASED TRAINING OF GAUSSIAN MIXTURE MODELS FOR HIGH-DIMENSIONAL STREAMING DATA

Anonymous authors
Paper under double-blind review

ABSTRACT

We present an approach for efficiently training Gaussian Mixture Models (GMMs) by Stochastic Gradient Descent (SGD) with non-stationary, high-dimensional streaming data. Our training scheme does not require data-driven parameter initialization (e.g., k-means) and has the ability to process high-dimensional samples without numerical problems. Furthermore, the approach allows mini-batch sizes as low as 1, typical for streaming-data settings, and it is possible to react and adapt to changes in data statistics (concept drift/shift) without catastrophic forgetting. Major problems in such streaming-data settings are undesirable local optima during early training phases, numerical instabilities due to high data dimensionalities, and catastrophic forgetting when encountering concept drift. We introduce an adaptive annealing procedure to address the first problem, which additionally plays a decisive role in controlling the GMMs' reaction to concept drift. Numerical instabilities are eliminated by using an exponential-free approximation to the standard GMM log-likelihood. By controlling the annealing parameter, the reaction to concept drift can be varied at a constant SGD learning rate (whose adaptation can lead to numerical and convergence issues). Experiments on a variety of visual and non-visual benchmarks show that our SGD approach can be trained completely without, for instance, k-means based centroid initialization, and compares to a favorably online variant of Expectation-Maximization (EM) – stochastic EM (sEM). Finally, we demonstrate superior performance of SGD-based training when compared to sEM when data statistics are subject to change.

1 INTRODUCTION

This contribution focuses Gaussian Mixture Models (GMMs), which represent a probabilistic unsupervised model for clustering and density estimation and allowing sampling and outlier detection. GMMs have been used in a wide range of scenarios, e.g., Melnykov & Maitra (2010). Commonly, free parameters of a GMM are estimated by using the Expectation-Maximizations (EMs) algorithm (Dempster et al., 1977), as it does not require learning rates and automatically enforces all GMM constraints. A popular online variant is stochastic Expectation Maximization (sEM) (Cappé & Moulines, 2009), which can be trained mini-batch wise and is, thus, more suited for large datasets or streaming data.

1.1 MOTIVATION

Intrinsically, EM is a batch-type algorithm. Memory requirements can therefore become excessive for large datasets. In addition, streaming-data scenarios require data samples to be processed one by one, which is impossible for a batch-type algorithm. Moreover, data statistics may be subject to changes over time (concept drift/shift), to which the GMM should adapt. In such scenarios, an online, mini-batch type of optimization such as SGD is attractive, as it can process samples one by one, has modest, fixed memory requirements and can adapt to changing data statistics.

1.2 RELATED WORK

Online EM is a technique for performing EM mini-batch wise, allowing to process large datasets. One branch of previous research Newton et al. (1986); Lange (1995); Chen et al. (2018) has been devoted to the development of stochastic Expectation Maximization (sEM) algorithms that reduce

the original EM method in the limit of large batch sizes. The variant of Cappé & Moulines (2009) is widely used due to its simplicity and efficiency for large datasets. These approaches come at the price of additional hyper-parameters (e.g., learning rate or mini-batch size), thus, removing a key advantage of EM over SGD. Another common approach is to modify the EM algorithm itself by, e.g., including heuristics for adding, splitting and merging centroids Vlassis & Likas (2002); Engel & Heinen (2010); Pinto & Engel (2015); Cederborg et al. (2010); Song & Wang (2005); Kristan et al. (2008); Vijayakumar et al. (2005). This allows GMM-like models to be trained by presenting one sample after another. The models work well in several application scenarios, but their learning dynamics are impossible to analyze mathematically. They also introduce a high number of parameters. Apart from these works, some authors avoid the issue of extensive datasets by determining smaller "core sets" of representative samples and performing vanilla EM Feldman et al. (2011).

SGD for training GMMs has, as far as we know, been recently treated only by Hosseini & Sra (2015; 2019). In this body of work, GMM constraint enforcement is ensured by using manifold optimization techniques and re-parameterization/regularization. Thereby, additional hyper-parameters are introduced. The issue of local optima is sidestepped by a k-means type centroid initialization, and the used image datasets are low-dimensional (36 dimensions). Additionally, enforcing positive definiteness constraints by Cholesky decomposition is discussed.

Annealing and Approximation approaches for GMMs were proposed by Verbeek et al. (2005); Pinheiro & Bates (1995); Ormoneit & Tresp (1998); Dognin et al. (2009). However, the regularizers proposed by Verbeek et al. (2005); Ormoneit & Tresp (1998) significantly differ from our scheme. GMM log-likelihood approximations, similar to the one used here, are discussed in, e.g., Pinheiro & Bates (1995) and Dognin et al. (2009), but only in combination with EM training.

GMM Training in High-Dimensional Spaces is discussed in several publications: A conceptually very interesting procedure is proposed by Ge et al. (2015). It exploits the properties of high-dimensional spaces in order to achieve learning with a number of samples that is polynomial in the number of Gaussian components. This is difficult to apply in streaming settings, since higher-order moments need to be estimated beforehand, and also because the number of samples usually cannot be controlled in practice. Training GMM-like lower-dimensional factor analysis models by SGD on high-dimensional image data is successfully demonstrated in Richardson & Weiss (2018), avoiding numerical issues, but, again, sidestepping the local optima issue by using k-means initialization. The numerical issues associated with log-likelihood computation in high-dimensional spaces are generally mitigated by using the "logsumexp" trick Nielsen & Sun (2016), which is, however, insufficient for ensuring numerical stability for particularly high-dimensional data, such as images.

1.3 Contributions

The main novel contributions of this article are:

- a proposal for numerically stable GMM training by SGD
- an automatic annealing procedure that ensures SGD convergence from a wide range of initial conditions without prior knowledge of the data (e.g., no k-means initialization) which is especially beneficial for high-dimensional data
- a novel and computationally efficient method for enforcing all GMM constraints in SGD
- a novel single-parameter mechanism for controlling a GMM's reaction to concept drift/shift

Apart from these contents, we provide a publicly available TensorFlow implementation.[1]

2 Datasets

We use a variety of different image-based datasets as well as a non-image dataset for evaluation purposes. All datasets are normalized to the $[0, 1]$ range.

MNIST (LeCun et al., 1998) contains gray scale images, which depict handwritten digits from 0 to 9 in a resolution of 28×28 pixels – the common benchmark for computer vision systems.

SVHN (Wang et al., 2012) contains color images of house numbers (0-9, resolution 32×32).

FashionMNIST (Xiao et al., 2017) contains gray scale images of 10 cloth categories and is considered as more challenging classification task compared to MNIST.

Fruits 360 (Murean & Oltean, 2018) consists of colored pictures showing different types of fruits ($100 \times 100 \times 3$ pixels). The ten best-represented classes are selected from this dataset.

[1] https://github.com/gmm-iclr21/sgd-gmm

Devanagari (Acharya et al., 2016) includes gray scale images of handwritten Devanagari letters with a resolution of 32×32 pixels – the first 10 classes are selected.
NotMNIST (Yaroslav Bulatov, 2011) is a gray scale image dataset (resolution 28×28 pixels) of letters from *A* to *J* extracted from different public available fonts.
ISOLET (Cole & Fanty, 1990) is a non-image dataset containing 7 797 samples of spoken letters recorded from 150 subjects. Each sample was encoded and is represented by 617 float values.

3 Gaussian Mixture Models

GMMs are probabilistic models that intend to explain the observed data $X = \{\boldsymbol{x}_n\}$ by expressing their density as a weighted mixture of K Gaussian component densities $\mathcal{N}(\boldsymbol{x}; \boldsymbol{\mu}_k, \boldsymbol{P}_k) \equiv \mathcal{N}_k(\boldsymbol{x})$: $p(\boldsymbol{x}) = \sum_k^K \pi_k \mathcal{N}_k(\boldsymbol{x})$. We work with precision matrices $\boldsymbol{P} = \boldsymbol{\Sigma}^{-1}$ instead of covariances $\boldsymbol{\Sigma}$. This is realized by optimizing the (incomplete) log-likelihood

$$\mathcal{L} = \mathbb{E}_n \left[\log \sum_k \pi_k \mathcal{N}_k(\boldsymbol{x}_n) \right]. \tag{1}$$

3.1 GMMs and SGD

GMMs require the mixture weights to be normalized: $\sum_k \pi_k = 1$ and the precision matrices to be positive definite: $\boldsymbol{x}^T \boldsymbol{P}_k \boldsymbol{x} \geq 0 \; \forall \boldsymbol{x}$. These constraints must be explicitly enforced after each SGD step:

Weights π_k are adapted according to Hosseini & Sra (2015), which replaces them by other free parameters ξ_k from which the π_k are computed so that normalization is ensured:

$$\pi_k = \frac{\exp(\xi_k)}{\sum_j \exp(\xi_j)}. \tag{2}$$

Precision Matrices need to be positive-definite, so we re-parameterize these as $\boldsymbol{P}_k = \left(\boldsymbol{D}_k^T \boldsymbol{D}_k\right)$, where the upper-diagonal matrices $\boldsymbol{D}_k$ result from a Cholesky decomposition. Consequently, $\det \boldsymbol{\Sigma}_k = \det \boldsymbol{P}_k^{-1} = \left(\det(\boldsymbol{D}_k^T \boldsymbol{D}_k)\right)^{-1} = \left(\operatorname{tr}(\boldsymbol{D}_k)\right)^{-2}$ can be computed efficiently. To avoid re-computing the costly Cholesky decomposition of the $\boldsymbol{P}_k$ at every iteration, we perform it on the initial precision matrices and just erase the elements below the diagonal in the $\boldsymbol{D}_k$ after each gradient step.

3.2 Max-Component Approximation for GMMs

The log-likelihood Eq. (1) is difficult to optimize by SGD (see Sec. 3.3). This is why we intend to find a lower bound that we can optimize instead. A simple scheme is given by

$$\mathcal{L} = \mathbb{E}_n \left[\log \sum_k \pi_k \mathcal{N}_k(\boldsymbol{x}_n) \right] \geq \mathbb{E}_n \left[\log \max_k \left(\pi_k \mathcal{N}_k(\boldsymbol{x}_n)\right) \right] = \hat{\mathcal{L}} = \mathbb{E}_n \left[\log \left(\pi_{k^*} \mathcal{N}_{k^*}(\boldsymbol{x}_n)\right) \right] \tag{3}$$

where $k^* = \arg\max_k \pi_k \mathcal{N}_k(\boldsymbol{x}_n)$. This is what we call the *max-component approximation* of Eq. (3). In contrast to the lower bound that is constructed for EM-type algorithms, this bound is usually not tight. The advantages of $\hat{\mathcal{L}}$ are the avoidance of local optima in SGD, and the elimination of exponentials causing numerical instabilities for high data dimensions. The "logsumexp" trick is normally employed with GMMs to rectify this by factoring out the largest component probability $\mathcal{N}_{k^*}$. This mitigates, but does not avoid numerical problems when distances are high. To give an example: we normalize the component probability $\mathcal{N}_k = e^{-101}$ (using 32-bit floats) by the highest probability $\mathcal{N}_{k^*} = e^3$, and we obtain $\frac{\mathcal{N}_k}{\mathcal{N}_{k^*}} = e^{-104}$, which is numerically problematic.

3.3 Undesirable Local Optima in SGD Training

An issue when performing SGD without k-means initialization concerns undesirable local optima.
Degenerate Solutions occur when naively optimizing $\mathcal{L}$ by SGD (see Fig. 1a). All components have the same weight, centroid and covariance matrix: $\pi_k \approx \frac{1}{K}$, $\boldsymbol{\mu}_k = \mathbb{E}[\boldsymbol{X}]$, $\boldsymbol{\Sigma}_k = \operatorname{Cov}(\boldsymbol{X}) \; \forall k$, in which case all gradients vanish (see App. A.3 for a proof). These solutions are avoided by $\hat{\mathcal{L}}$, since only a

subset of components is updated by SGD, thereby breaking the symmetry between components.

Single/Sparse-Component Solutions occur when optimizing $\hat{\mathcal{L}}$ by SGD (see Fig. 1b). They are characterized by one or several components $\{k_i\}$ that have large weights with centroid and precision matrices given by the mean and covariance of a significant subset $\boldsymbol{X}_{k_i} \subset \boldsymbol{X}$ of the data $\boldsymbol{X}$: $\pi_{k_i} \gg 0$, $\boldsymbol{\mu}_{k_i} = \mathbb{E}[\boldsymbol{X}_{k_i}]$, $\boldsymbol{\Sigma}_{k_i} = \mathrm{Cov}(\boldsymbol{X}_{k_i})$, whereas the remaining components k are characterized by $\pi_k \approx 0$, $\boldsymbol{\mu}_k = \boldsymbol{\mu}(t=0)$, $\boldsymbol{P}_k = \boldsymbol{P}(t=0)$. Thus, these unconverged components are almost never best-matching components k^*. The max-operation in $\hat{\mathcal{L}}$ causes gradients like $\frac{\partial \hat{\mathcal{L}}}{\partial \boldsymbol{\mu}_k}$ to contain δ_{kk^*} (see App. A.3). This implies that they are non-zero only for the best-matching component k^*. Thus the gradients of unconverged components vanish, implying that they remain in their unconverged state.

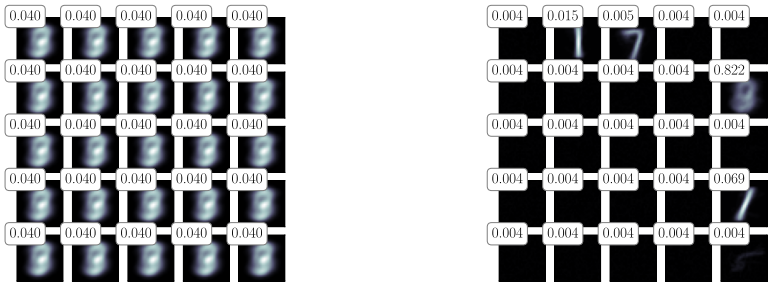

a) degenerate solution (optimizing $\mathcal{L}$) b) sparse-component solution (optimizing $\hat{\mathcal{L}}$)

Figure 1: Undesirable solutions during SGD, visualized for MNIST with component weights π_k.

3.4 Annealing Procedure for Avoiding Local Optima

Our approach for avoiding undesirable solutions is to punish their characteristic response patterns by a modification of $\hat{\mathcal{L}}$, the *smoothed max-component log-likelihood* $\hat{\mathcal{L}}^\sigma$:

$$\hat{\mathcal{L}}^\sigma = \mathbb{E}_n \max_k \left[\sum_j \boldsymbol{g}_{kj}(\sigma) \log \Big(\pi_j \mathcal{N}_j(\boldsymbol{x}_n) \Big) \right] = \mathbb{E}_n \sum_j \boldsymbol{g}_{k^*j}(\sigma) \log \Big(\pi_j \mathcal{N}_j(\boldsymbol{x}_n) \Big). \tag{4}$$

The entries of the $\boldsymbol{g}_k$ are computed by a Gaussian function centered on component k with common spatial standard deviation σ, where we assume that the K components are arranged on a $\sqrt{K} \times \sqrt{K}$ grid with 2D Euclidean metric (see App. A.5). Eq. (4) essentially represents a smoothing of the $\log(\pi_k \mathcal{N}_k(\boldsymbol{x}))$ with a 2D convolution filter (we use periodic boundary conditions). Thus, Eq. (4) is maximized if the log probabilities follow a uni-modal Gaussian profile of spatial variance $\sim \sigma^2$, which heavily punishes single-component solutions that have a locally delta-like response.

Annealing starts with large values of $\sigma(t) = \sigma_0$ and reduces it over time to an asymptotic small value of $\sigma = \sigma_\infty$, thus, smoothly transitioning from $\hat{\mathcal{L}}^\sigma$ in Eq. (4) into $\hat{\mathcal{L}}$ in Eq. (3).

Annealing Control is ensured by adjusting σ, which defines an effective upper bound on $\hat{\mathcal{L}}^\sigma$ (see App. A.2 for a proof). This implies that the loss will be stationary once this bound is reached, which we consider a suitable indicator for reducing σ. We implement an annealing control that sets $\sigma \leftarrow 0.9\sigma$ whenever the loss is considered sufficiently stationary. Stationarity is detected by maintaining an exponentially smoothed average $\ell(t) = (1-\alpha)\ell(t-1) + \alpha \hat{\mathcal{L}}^\sigma(t)$ on time scale α. Every $\frac{1}{\alpha}$ iterations, we compute the fractional increase of $\hat{\mathcal{L}}^\sigma$ as

$$\Delta = \frac{\ell(t) - \ell(t - \alpha^{-1})}{\ell(t - \alpha^{-1}) - \hat{\mathcal{L}}^\sigma(t=0)} \tag{5}$$

and consider the loss stationary iff $\Delta < \delta$ (the latter being a free parameter). The choice of the time constant for smoothing $\hat{\mathcal{L}}^\sigma$ is outlined in the following section.

3.5 Training Procedure for SGD

Training GMMs with SGD is performed by maximizing the smoothed max-component log-likelihood $\hat{\mathcal{L}}^\sigma$ from Eq. (4). At the same time, we enforce the constraints on the component weights and

covariances as described in Sec. 3.1 and transition from $\hat{\mathcal{L}}^{\sigma}$ into $\hat{\mathcal{L}}$ by annealing (see Sec. 3.4). SGD requires a learning rate ϵ to be set, which in turn determines the parameter α (see Sec. 3.4) as $\alpha = \epsilon$ since stationarity detection should operate on a time scale similar to that of SGD. Cholesky matrices $\boldsymbol{D}_k$ are initialized to $D_{\text{max}} I$ and are clipped after each iteration so that diagonal entries are in the range $[0, D_{\text{max}}^2]$. This is necessary to avoid excessive growth of precisions for data entries with vanishing variance, e.g., pixels that are always black. Weights are uniformly initialized to $\pi^i = \frac{1}{K}$, centroids in the range $[-\mu^i, +\mu^i]$ (see Alg. 1 for a summary). Please note that our SGD approach requires no centroid initialization by k-means, as it is usually recommended when training GMMs with EM. We discuss and summarize good practices for choosing hyper-parameters Sec. 5.

Algorithm 1: Steps of SGD-GMM training.

Data: initializer values: μ^i, K, $\epsilon_0/\epsilon_\infty$, σ_0/σ_∞, δ and data $\boldsymbol{X}$
Result: trained GMM model

$\boldsymbol{\mu} \leftarrow \mathcal{U}(-\mu^i, +\mu^i)$, $\pi \leftarrow 1/K$, $\boldsymbol{P} \leftarrow I D_{\text{max}}$, $\sigma \leftarrow \sigma_0$, $\epsilon \leftarrow \epsilon_0$ // initialize
forall $\boldsymbol{x} \in \boldsymbol{X}$ **do** // or mini-batches
  $\boldsymbol{g} \leftarrow$ create_annealing_mask(σ) // see App. A.5 for more details
  $\pi \leftarrow$ normalization(π) // see Eq. (2)
  $\boldsymbol{\mu}, \boldsymbol{P}, \pi \leftarrow \epsilon \frac{\partial \hat{\mathcal{L}}^{\sigma}}{\partial \boldsymbol{\mu}} + \boldsymbol{\mu}, \epsilon \frac{\partial \hat{\mathcal{L}}^{\sigma}}{\partial \boldsymbol{P}} + \boldsymbol{P}, \epsilon \frac{\partial \hat{\mathcal{L}}^{\sigma}}{\partial \pi} + \pi$ // update by gradients
  $\boldsymbol{P} \leftarrow$ prec_clipping($\boldsymbol{P}$, D_{max})
  $\ell \leftarrow (1-\alpha)\ell + \alpha \hat{\mathcal{L}}^{\sigma}(\boldsymbol{x})$ // sliding log-likelihood
  if *annealing update iteration* **then**
    if $\Delta < \delta$ **then** $\sigma \leftarrow 0.9\sigma$, $\epsilon \leftarrow 0.9\epsilon$ // Δ see Eq. (5)

3.6 Training Procedure for stochastic Expectation Maximization

We use sEM as proposed by Cappé & Moulines (2009). We choose the step size of the form $\rho_t = \rho_0 (t+1)^{-0.5+\alpha}$, with $\alpha \in [0, 0.5]$, $\rho_0 < 1$ and enforce $\rho(t) \geq \rho_\infty$. Values for these parameters are determined via a grid search in the ranges $\rho_0 \in \{0.01, 0.05, 0.1\}$, $\alpha \in \{0.01, 0.25, 0.5\}$ and $\rho_\infty \in \{0.01, 0.001, 0.0001\}$. Each sEM iteration uses a batch size B. Initial accumulation of sufficient statics is conducted for 10% of an epoch, but not when re-training with new data statistics. Parameter initialization and clipping of precisions is performed just as for SGD, see Sec. 3.5.

3.7 Comparing SGD and sEM

Since sEM optimizes the log-likelihood $\mathcal{L}$, whereas SGD optimizes the annealed approximation $\hat{\mathcal{L}}^{\sigma}$, the comparison of these measures should be considered carefully. We claim that the comparison is fair assuming that **i)** SGD annealing has converged and **ii)** GMM responsibilities are sharply peaked so that a single component has responsibility of ≈ 1. It follows from **i)** that $\hat{\mathcal{L}}^{\sigma} \approx \hat{\mathcal{L}}$ and **ii)** implies that $\hat{\mathcal{L}} \approx \mathcal{L}$. Condition **ii)** is usually satisfied to high precision especially for high-dimensional inputs: if it is not, the comparison is biased in favor of sEM, since $\mathcal{L} > \hat{\mathcal{L}}$ by definition.

4 Experiments

Unless stated otherwise, the experiments in this section will be conducted with the following parameter values for sEM and SGD (where applicable): mini-batch size $B = 1$, $K = 8 \times 8$, $\mu^i = 0.1$, $\sigma_0 = 2$, $\sigma_\infty = 0.01$, $\epsilon = 0.001$, $D_{\text{max}} = 20$. Each experiment is repeated 10 times with identical parameters. See Sec. 5 for a justification of these choices. Due to input dimensionality, all precision matrices must be taken to be diagonal. Training/test data are taken from the datasets mentioned in Sec. 2.

4.1 Robustness of SGD to Initial Conditions

Here, we train GMMs for three epochs on classes 1 to 9 for each dataset. We use different random and non-random initializations of the centroids and compare the final log-likelihood values. Random centroid initializations are parameterized by $\mu^i \in \{0.1, 0.3, 0.5\}$, whereas non-random initializations are defined by centroids from a previous training run on class 0 (one epoch). The latter is done to

have a non-random centroid initialization that is as dissimilar as possible from the training data. The initialization of the precisions cannot be varied because empirical data shows that training converges to undesirable solutions if the precisions are not initialized to large values. While this will have to be investigated further, we find that convergence to near-identical levels, regardless of centroid initialization for all datasets (see Tab. 1 for more details).

Table 1: Effect of different random and non-random centroid initializations of SGD training. Given are the means and standard deviations of final log-likelihoods (10 repetitions per experiment).

Initialization	**random**						**non-random**	
	$\mu^i = 0.1$		$\mu^i = 0.3$		$\mu^i = 0.5$		init class 0	
Dataset	$mean$	std	$mean$	std	$mean$	std	$mean$	std
MNIST	205.47	1.08	205.46	0.77	205.68	0.78	205.37	0.68
FashionMNIST	231.22	1.53	231.58	2.84	231.00	1.11	229.59	0.59
NotMNIST	−48.41	1.77	−48.59	1.56	−48.32	1.13	−49.37	2.32
Devanagari	−15.95	1.59	−15.76	1.34	−17.01	1.11	−22.07	4.59
Fruits 360	12 095.80	98.02	12 000.70	127.00	12 036.25	122.06	10 912.79	1 727.61
SVHN	1 328.06	0.94	1 327.99	1.59	1 328.40	1.17	1 327.80	0.94
ISOLET	354.34	0.04	354.36	0.04	354.36	0.04	354.20	0.05

4.2 Clustering Performance Evaluation

To compare the clustering performance of sEM and GMM the Davies-Bouldin score (Davies & Bouldin, 1979) and the Dunn index (Dunn, 1973) are determined. Both metrics use the assigned cluster center ids to measure the clustering capabilities. We evaluate the grid-search results to find the best parameter setup for each metric for comparison. sEM is initialized by k-means to show that our approach do not depend on initialization parameters. To keep to computational cost of the computed metrics low $1\,000$ test samples per measurement point are used. The mean of the last measuring point over 10 experiment repetitions is used to find the best experiments – as low as possible for Davies-Bouldin score and a higher Dunn index indicates better clustering. Tab. 2 show the results for each individual metric, model and dataset. In App. A.6 the trend during the training phase is shown.

Table 2: Clustering performance comparison of SGD and sEM training. Used metrics are Davies-Bouldin score (less is better) and Dunn index (more is better). Each time mean metric value (of 10 experiment repetitions) at the end of training, and their standard deviations are presented. Results are in bold face whenever they are better by more than half a standard deviation.

Metric / Algo.	**Davies-Bouldin score**				**Dunn index**			
	SGD		**sEM**		**SGD**		**sEM**	
Dataset	$mean$	std	$mean$	std	$mean$	std	$mean$	std
MNIST	2.50	0.04	**2.47**	0.04	0.18	0.02	0.16	0.02
FashionMNIST	**2.06**	0.05	2.20	0.04	0.20	0.03	0.19	0.02
NotMNIST	2.30	0.03	**2.12**	0.03	0.15	0.03	0.14	0.04
Devanagari	**2.60**	0.04	2.64	0.02	**0.33**	0.01	0.27	0.04
SVHN	**2.34**	0.04	2.41	0.03	0.15	0.02	0.15	0.02

4.3 Streaming-Data Experiments with Constant Data Statistics

We train GMMs for three epochs using SGD and sEM on all datasets as described in Secs. 3.5 and 3.6.The resulting centroids of our SGD-based approach are shown in Fig. 2, whereas the final loss values for SGD and sEM are compared in Tab. 3. The centroids for both approaches are visually similar, except for the topological organization due to annealing for SGD, and the fact that in most experiments, some components do not converge for sEM while the others do. Tab. 3 indicates that SGD achieves performances superior to sEM in the majority of cases, in particular for the highest-dimensional datasets (SVHN: $3\,072$ dimensions and Fruits 360: $30\,000$ dimensions).

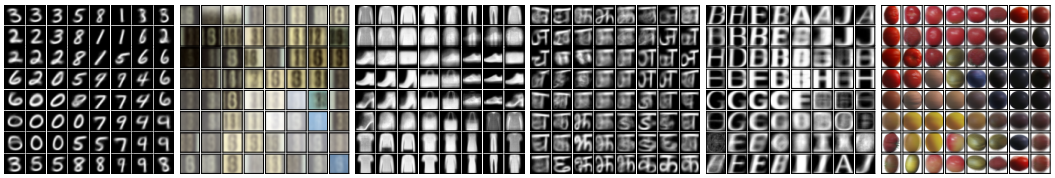

MNIST SVHN FashionMNIST Devanagari NotMNIST Fruits 360

Figure 2: Exemplary results for centroids learned by SGD, trained on full images.

Table 3: Comparison of SGD and sEM training on all datasets in a streaming-data scenario. Each time mean log-likelihoods (10 repetitions) at the end of training, and their standard deviations are presented. Results are in bold face whenever they are higher by more than half a standard deviation.

Algorithm / Dataset	**SGD**		**sEM**	
	mean	*std*	*mean*	*std*
MNIST	216.60	0.31	216.82	1.38
FashionMNIST	**234.59**	2.28	222.95	6.03
NotMNIST	**−34.76**	1.16	−40.09	8.90
Devanagari	**−14.65**	1.09	−13.46	6.16
Fruits 360	**11754.32**	75.63	5 483.00	1 201.60
SVHN	**1329.83**	0.80	1 176.07	16.91
ISOLET	354.21	0.01	354.55	0.37

4.4 Concept Drift Experiments

We perform a sequential learning task consisting of three successive, class-disjoint sub-tasks. Training is conducted on sub-task D_1 (classes 1-8), subsequently on D_2 (class 0) and then on D_3 (class 9). In order to measure forgetting, we record the log-likelihood computed on $D_1 \cup D_2 \cup D_3$ (summarized to D_{All}) after the last training step of D_3.

On each sub-task, training is performed for $\mathcal{E} = 2$ epochs. sEM parameters (see Sec. 3.6) are fixed by a grid-search on D_1. The only SGD parameter that is varied is the annealing radius (set to 2.0 at the start of D_1), which is re-set at the start of sub-tasks D_2 and D_3 to values of $\sigma_0 \in \{0.01, 0.3, 0.5\}$.

The results can be viewed in Tab. 4. They show, on the one hand, that the value of σ_0 at the start of each sub-task controls forgetting, where large values lead to fast adaptation and fast forgetting. This is intuitive, as σ defines how many components adjacent to the best matching unit (BMU) are adapted in a single iteration. On the other hand, we observe that a suitable choice of σ_0 at the start of D_2 and D_3 makes SGD strongly superior to sEM in terms of re-learning and retention (see also App. A.7).

Table 4: Effect of different re-initializations of σ_0 when learning under concept drift for SGD compared to sEM. The means and standard deviations over 10 repetitions are shown. Results are in bold face whenever they are higher by more than half a standard deviation.

Algorithm / Dataset	**SGD**						**sEM**	
	$\sigma_0 = 0.01$		$\sigma_0 = 0.3$		$\sigma_0 = 0.5$			
	mean	*std*	*mean*	*std*	*mean*	*std*	*mean*	*std*
MNIST	206.36	0.56	205.61	0.84	188.76	2.13	206.02	2.19
FashionMNIST	**221.19**	1.21	220.10	1.10	184.04	5.44	205.97	4.82
NotMNIST	**−115.81**	6.25	−117.55	6.74	−192.74	17.71	−302.02	11.47
Devanagari	**−28.17**	1.21	−28.27	2.14	−35.71	2.44	−47.42	10.70
Fruits 360	**11243.71**	156.62	11 265.83	156.62	11 265.83	114.43	2 529.21	1 844.93
SVHN	**1312.05**	2.28	1 312.46	1.68	1 290.21	1.68	1 156.46	23.06
ISOLET	354.82	0.01	354.80	0.01	354.51	0.01	354.54	0.35

5 Discussion and Conclusion

The **Relevance of this Article** is outlined by the fact that training GMMs by SGD was recently investigated in the community by Hosseini & Sra (2015; 2019). We go beyond, since our approach does not rely on off-line data-driven model initialization, and works for high-dimensional streaming data, while allowing to control forgetting in concept drift situations. The presented SGD scheme is simple to implement and very robust to initial conditions due to the proposed annealing procedure, see Sec. 4.1. In addition, our SGD approach compares favorably to the reference model for online EM (Cappé & Moulines, 2009) in terms of achieved log-likelihoods, which was verified on multiple real-world datasets. Superior SGD performance is observed for the high-dimensional datasets.

Analysis of Results suggests that SGD performs better than sEM on average, see Sec. 4.3, although the differences are modest on average. If sEM is used without a valid initialization (e.g., k-means), it happens, especially with high-dimensional data (Fruits 360 and SVHN datasets), that components do not converge (see App. A.4 for a visual impression). Another important advantage of SGD over sEM is the fact that no grid search for finding certain hyper-parameter values is necessary, whereas sEM has a complex and unintuitive dependency on ρ_0, ρ_∞ and α_0.

Incremental Learning and Annealing experiments in Sec. 4.4 show that changes in data statistics do not lead to catastrophic, but gradual forgetting, both for SGD and sEM, although SGD performs markedly better in this comparison. It is plausible that our SGD approach is superior to sEM because sEM updates all components for every sample, whereas SGD updates only a neighborhood (controlled by σ) around the best-matching one. Thus, if a sample is similar to several components, only one component is modified, which reduces forgetting. The size of this neighborhood is controlled by specific settings of the parameter σ_0, which explains its role in controlling forgetting.

Small Batch Sizes and Streaming Data are possible with the SGD-based approach. Throughout the experiments, we used a batch size of 1, which allows streaming-data processing without the need to store any samples at all. Larger batch sizes are, of course, possible and increase execution speed. In the experiments conducted here, SGD (and sEM) usually converged within the first two epochs, which is a substantial advantage whenever huge sets of data have to be processed.

No Assumptions About Data Generation are made by SGD in contrast to the EM and sEM algorithms. The latter guarantee that the loss will not decrease due to an M-step. This, however, assumes a non-trivial dependency of the data on an unobservable latent variable (see App. A.1 for a proof). In contrast, SGD makes no such hard-to-verify assumptions, which is a rather philosophical point, but may be an advantage in certain situations where data are strongly non-Gaussian.

Numerical Stability is assured by our SGD training approach. It does not optimize the log-likelihood but its max-component approximation, which contains no exponentials at all. In fact, it is the gradient computations where numerical problems (e.g., NaN values) occurred. The "logsumexp" trick mitigates the problem, but does not eliminate it (see Sec. 3.2). It cannot be used when gradients are computed automatically (what most machine learning frameworks do).

Hyper-Parameter Selection Guidelines are as follows: the learning rate ϵ must be set by cross-validation or repeated runs (a good value is 0.001). We empirically found that initializing precisions to the cut-off value D_{max} and an uniform initialization of the π_i are beneficial, and that centroids are best initialized to small random values. A value of $D_{\text{max}} = 20$ always worked in the experiments. Generally, the cut-off must be much larger than than the inverse of the data variance. In many cases, it should be possible to estimate this roughly, even in streaming settings, especially when samples are normalized. The number of components K should be as large as possible – more is always better. The parameter δ controls loss stationarity detection for the annealing procedure and was shown to perform well for $\delta = 0.05$. Larger values will lead to faster decrease of $\sigma(t)$, which may impair convergence. Smaller values are always admissible but lead to longer convergence times. The annealing time constant α should be set to the GMM learning rate ϵ or lower. Smaller values of α lead to longer convergence times since $\sigma(t)$ will be updated less often. The initial value σ_0 needs to be large in order to enforce convergence for all components. A typical value is $0.25\sqrt{K}$. The lower bound on σ, σ_∞ should be as small as possible to achieve high log-likelihoods (e.g., 0.01, see proof in App. A.2).

Computing Infrastructure used for the experiments was 30 off-the-shelf PCs, each equipped with a Nvidia GeForce RTX 2060 GPU. Due to small mini-batch sizes, an SGD experiment (three epochs on MNIST) takes about 5 minutes. For mini-batch sizes of 100, the same experiment takes about 20s.

6 OUTLOOK

The presented work can be extended in several ways: First of all, annealing control could be simplified further by inferring good δ values from α. Likewise, *increases* of σ might be performed automatically when the loss rises sharply, indicating a task boundary. As we found that GMM convergence times grow linear with the number of components, we will investigate hierarchical GMM models that operate like a Convolutional Neural Network (CNN), and in which individual GMMs only see a local patch of the input and can therefore have low K. Lastly, we will investigate a replay by SGD-trained GMMs for continual learning architectures. GMMs could compare favorably to Generative Adversarial Nets (Goodfellow et al., 2014) due to faster training and the fact that sample generation capacity can be monitored via the log-likelihood.

REFERENCES

Shailesh Acharya, Ashok Kumar Pant, and Prashnna Kumar Gyawali. Deep learning based large scale handwritten Devanagari character recognition. *SKIMA 2015 - 9th International Conference on Software, Knowledge, Information Management and Applications*, 2016. doi: 10.1109/SKIMA.2015.7400041.

Olivier Cappé and Eric Moulines. On-line expectation-maximization algorithm for latent data models. *Journal of the Royal Statistical Society. Series B: Statistical Methodology*, 71(3):593–613, 2009. ISSN 13697412. doi: 10.1111/j.1467-9868.2009.00698.x.

Thomas Cederborg, Ming Li, Adrien Baranes, and Pierre Yves Oudeyer. Incremental local online Gaussian Mixture Regression for imitation learning of multiple tasks. *IEEE/RSJ 2010 International Conference on Intelligent Robots and Systems, IROS 2010 - Conference Proceedings*, pp. 267–274, 2010. doi: 10.1109/IROS.2010.5652040.

Jianfei Chen, Jun Zhu, Yee Whye Teh, and Tong Zhang. Stochastic expectation maximization with variance reduction. *Advances in Neural Information Processing Systems*, 2018-December (NeurIPS):7967–7977, 2018. ISSN 10495258.

Ronald Cole and Mark Fanty. Spoken letter recognition. pp. 385–390, 1990. doi: 10.3115/116580.116725.

David L. Davies and Donald W. Bouldin. A Cluster Separation Measure. *IEEE Transactions on Pattern Analysis and Machine Intelligence*, PAMI-1(2):224–227, 1979. ISSN 01628828. doi: 10.1109/TPAMI.1979.4766909.

A. P. Dempster, N. M. Laird, and D. B. Rubin. Maximum Likelihood from Incomplete Data Via the EM Algorithm . *Journal of the Royal Statistical Society: Series B (Methodological)*, 39(1):1–22, 1977. doi: 10.1111/j.2517-6161.1977.tb01600.x.

Pierre L. Dognin, Vaibhava Goel, John R. Hershey, and Peder A. Olsen. A fast, accurate approximation to log likelihood of Gaussian mixture models. *ICASSP, IEEE International Conference on Acoustics, Speech and Signal Processing - Proceedings*, (3):3817–3820, 2009. ISSN 15206149. doi: 10.1109/ICASSP.2009.4960459.

J. C. Dunn. A fuzzy relative of the ISODATA process and its use in detecting compact well-separated clusters. *Journal of Cybernetics*, 3(3):32–57, 1973. ISSN 00220280. doi: 10.1080/01969727308546046.

Paulo Martins Engel and Milton Roberto Heinen. Incremental learning of multivariate Gaussian mixture models. *Lecture Notes in Computer Science (including subseries Lecture Notes in Artificial Intelligence and Lecture Notes in Bioinformatics)*, 6404 LNAI:82–91, 2010. ISSN 03029743. doi: 10.1007/978-3-642-16138-4_9.

Dan Feldman, Matthew Faulkner, and Andreas Krause. Scalable training of mixture models via coresets. *Advances in Neural Information Processing Systems 24: 25th Annual Conference on Neural Information Processing Systems 2011, NIPS 2011*, pp. 1–9, 2011.

Rong Ge, Qingqing Huang, and Sham M. Kakade. Learning mixtures of gaussians in high dimensions. *Proceedings of the Annual ACM Symposium on Theory of Computing*, 14-17-June-2015:761–770, 2015. ISSN 07378017. doi: 10.1145/2746539.2746616.

Ian Goodfellow, Jean Pouget-Abadie, Mehdi Mirza, Bing Xu, David Warde-Farley, Sherjil Ozair, Aaron Courville, and Yoshua Bengio. Generative adversarial nets. In Z. Ghahramani, M. Welling, C. Cortes, N. D. Lawrence, and K. Q. Weinberger (eds.), *Advances in Neural Information Processing Systems 27*, pp. 2672–2680. Curran Associates, Inc., 2014. URL `http://papers.nips.cc/paper/5423-generative-adversarial-nets.pdf`.

Reshad Hosseini and Suvrit Sra. Matrix manifold optimization for Gaussian mixtures. *Advances in Neural Information Processing Systems*, 2015-January:910–918, 2015. ISSN 10495258.

Reshad Hosseini and Suvrit Sra. An alternative to em for gaussian mixture models: Batch and stochastic riemannian optimization. *Mathematical Programming*, pp. 1–37, 2019.

Matej Kristan, Danijel Skocaj, and Aleš Leonardis. Incremental learning with gaussian mixture models. In *Computer Vision Winter Workshop*, pp. 25–32, 2008.

Kenneth Lange. A Gradient Algorithm Locally Equivalent to the EM Algorithm. *Journal of the Royal Statistical Society: Series B (Methodological)*, 57(2):425–437, 1995. ISSN 0035-9246. doi: 10.1111/j.2517-6161.1995.tb02037.x.

Yann LeCun, Léon Bottou, Yoshua Bengio, and Patrick Haffner. Gradient-based learning applied to document recognition. *Proceedings of the IEEE*, 86(11):2278–2323, 1998. ISSN 00189219. doi: 10.1109/5.726791. URL `http://ieeexplore.ieee.org/document/726791`.

Volodymyr Melnykov and Ranjan Maitra. Finite mixture models and model-based clustering. *Statistics Surveys*, 4(October):80–116, 2010. ISSN 19357516. doi: 10.1214/09-SS053.

Horea Murean and Mihai Oltean. Fruit recognition from images using deep learning. *Acta Universitatis Sapientiae, Informatica*, 10(1):26–42, 2018. ISSN 2066-7760. doi: 10.2478/ausi-2018-0002. URL `http://arxiv.org/abs/1712.00580`.

J. Newton, D. M. Titterington, A. F. M. Smith, and U. E. Makov. Statistical Analysis of Finite Mixture Distributions. *Biometrics*, 42(3):679, 1986. ISSN 0006341X. doi: 10.2307/2531224.

Frank Nielsen and Ke Sun. Guaranteed bounds on information-theoretic measures of univariate mixtures using piecewise log-sum-exp inequalities. *Entropy*, 18(12), 2016. ISSN 10994300. doi: 10.3390/e18120442.

Dirk Ormoneit and Volker Tresp. Averaging, maximum penalized likelihood and Bayesian estimation for improving Gaussian mixture probability density estimates. *IEEE Transactions on Neural Networks*, 9(4):639–650, 1998. ISSN 10459227. doi: 10.1109/72.701177.

Jose C. Pinheiro and Douglas M. Bates. Approximations to the log-likelihood function in the nonlinear mixed-effects model. *Journal of Computational and Graphical Statistics*, 4(1):12–35, 1995. ISSN 15372715. doi: 10.1080/10618600.1995.10474663.

Rafael Coimbra Pinto and Paulo Martins Engel. A fast incremental Gaussian mixture model. *PLoS ONE*, 10(10), 2015. ISSN 19326203. doi: 10.1371/journal.pone.0139931.

Eitan Richardson and Yair Weiss. On GANs and GMMs. *Advances in Neural Information Processing Systems*, 2018-December(NeurIPS):5847–5858, 2018. ISSN 10495258.

Mingzhou Song and Hongbin Wang. Highly efficient incremental estimation of Gaussian mixture models for online data stream clustering. *Intelligent Computing: Theory and Applications III*, 5803:174, 2005. doi: 10.1117/12.601724.

J. J. Verbeek, N. Vlassis, and B. J.A. Kröse. Self-organizing mixture models. *Neurocomputing*, 63 (SPEC. ISS.):99–123, 2005. ISSN 09252312. doi: 10.1016/j.neucom.2004.04.008.

Sethu Vijayakumar, Aaron D'Souza, and Stefan Schaal. Incremental online learning in high dimensions. *Neural Computation*, 17(12):2602–2634, 2005. ISSN 08997667. doi: 10.1162/089976605774320557.

Nikos Vlassis and Aristidis Likas. A greedy EM algorithm for Gaussian mixture learning. *Neural Processing Letters*, 15(1):77–87, 2002. ISSN 13704621. doi: 10.1023/A:1013844811137.

Tao Wang, David J Wu, Adam Coates, and Andrew Y Ng. End-to-end text recognition with convolutional neural networks. In *Proceedings of the 21st International Conference on Pattern Recognition (ICPR2012)*, pp. 3304–3308. IEEE, 2012.

Han Xiao, Kashif Rasul, and Roland Vollgraf. Fashion-MNIST: a Novel Image Dataset for Benchmarking Machine Learning Algorithms. pp. 1–6, 2017. URL `http://arxiv.org/abs/1708.07747`.

Yaroslav Bulatov. Machine Learning, etc notMNIST dataset, 2011. URL `http://yaroslavvb.blogspot.com.br/2011/09/notmnist-dataset.html`.

A SUPPLEMENTARY MATERIAL

A.1 ASSUMPTIONS MADE BY EM AND SGD

The EM algorithm assumes that the observed data samples $\{\boldsymbol{x}_n\}$ depend on unobserved latent variables $\boldsymbol{z}_n$ in a non-trivial fashion. This assumption is formalized for a GMM with K components by formulating the complete-data likelihood in which $\boldsymbol{z}_n \equiv z_n \in \{0, \dots, K-1\}$ is a scalar:

$$p(\boldsymbol{x}_n, z_n) = \pi_{z_n} \mathcal{N}_{z_n}(\boldsymbol{x}_n) \tag{6}$$

where we have defined $\mathcal{N}_k(\boldsymbol{x}_n) = \mathcal{N}(\boldsymbol{x}_n; \boldsymbol{\theta}_k, \boldsymbol{\mu}_k)$ for brevity. It is assumed that the z_n are unobservable random variables whose distribution is unknown. Marginalizing them out gives us the incomplete-data likelihood $p(\boldsymbol{x}_n) = \sum_k p(\boldsymbol{x}_n, z_n)$. The derivation of the EM algorithm starts out with the total incomplete-data log-likelihood

$$\begin{aligned}
\mathcal{L} &= \log p(X) \\
&= \log \prod_n p(\boldsymbol{x}_n) \\
&= \sum_n \log p(\boldsymbol{x}_n) \\
&= \sum_n \log \sum_k p(\boldsymbol{x}_n, z_n = k) \\
&= \sum_n \log \sum_k p(z_n = k) \frac{p(\boldsymbol{x}_n, z_n = k)}{p(z_n = k)}.
\end{aligned} \tag{7}$$

Due to the assumption that $\mathcal{L}$ is obtained by marginalizing out the latent variables, an explicit dependency on z_n can be re-introduced. For the last expression, Jensen' inequality can be used to construct a lower bound:

$$\begin{aligned}
\mathcal{L} =& \sim \sum_n \log \sum_k p(\boldsymbol{z}_n = k) \frac{p(\boldsymbol{x}_n, \boldsymbol{z}_n = k)}{p(\boldsymbol{z}_n = k)} \\
&\geq \sum_n \sum_k p(\boldsymbol{z}_n = k) \log \frac{p(\boldsymbol{x}_n, \boldsymbol{z}_n = k)}{p(\boldsymbol{z}_n = k)}.
\end{aligned} \tag{8}$$

Since the realizations of the latent variables are unknown, we can assume any form for their distribution. In particular, for the choice $p(z_n) \sim p(\boldsymbol{x}_n, z_n)$, the lower bound becomes tight. Simple algebra and the fact that the distribution $p(z_n)$ must be normalized gives us:

$$\begin{aligned}
p(z_n = k) &= \frac{p(z_n = k, \boldsymbol{x}_n)}{p(\boldsymbol{x}_n)} \\
&= p(z_n = k | \boldsymbol{x}_n) \\
&= \frac{p(z_n = k, \boldsymbol{x}_n)}{\sum_l p(z_n = l, \boldsymbol{x}_n)} \\
&= \frac{\pi_k \mathcal{N}_k(\boldsymbol{x}_n)}{\sum_l \pi_l \mathcal{N}_l(\boldsymbol{x}_n)}
\end{aligned} \tag{9}$$

where we have used Eq. (6) in the last step. $p(z_n = k | \boldsymbol{x}_n)$ is a quantity that can be computed from data with no reference to the latent variables. For GMMs it is usually termed *responsibility* and we write it as $p(z_n = k | \boldsymbol{x}_n) \equiv \gamma_{nk}$.

However, the construction of a tight lower bound, which is actually different from $\mathcal{L}$, only works when $p(\boldsymbol{x}_n, z_n)$ depends non-trivially on the latent variable z_n. If this is not the case, we have

$p(\boldsymbol{x}_n, z_n) = K^{-1} p(\boldsymbol{x}_n)$ and the derivation of Eq. (8) develops down very differently:

$$\begin{aligned}
\mathcal{L} \sim \sum_n \log p(\boldsymbol{x}_n) &\geq \sum_n \sum_k p(z_n = k) \log \frac{p(\boldsymbol{x}_n, z_n = k)}{p(z_n = k)} \\
&= \sum_n \sum_k p(z_n = k) \log \frac{K^{-1} p(\boldsymbol{x}_n)}{p(z_n = k)} \\
&= \sum_n \log \Big(K^{-1} p(\boldsymbol{x}_n) \Big) - \sum_k p(z_n = k) \log p(z_n = k) \\
&\equiv \sum_n \Big(\log p(\boldsymbol{x}_n) - \big(\log K - \mathcal{H}[z_n] \big) \Big)
\end{aligned} \tag{10}$$

where $\mathcal{H}$ represents the Shannon entropy of $p(\boldsymbol{z})$. The highest value this can have is $\log K$ for an uniform distribution of the z_n, finally leading to a lower bound for $\mathcal{L}$ of

$$\mathcal{L} \geq \sum_n \Big(\log p(\boldsymbol{x}_n) \Big) = \mathcal{L} \tag{11}$$

which is indeed tight, but trivial, and thus does not simplify the problem at all. In particular, no closed-form solutions to the associated extreme value problem can be computed for this case.

This shows that optimizing GMMs by Expectation-Maximization assumes that each sample has been drawn from a single element in a set of K uni modal Gaussian distributions. Which distribution is selected for sampling depends on a latent random variable. On the other hand, optimization by SGD uses the incomplete-data log-likelihood $\mathcal{L}$ as basis for optimization, without probabilistic interpretation. This may be advantageous for problems where the assumption of Gaussianity is badly violated, although empirical studies indicate that optimization by EM works very well in a wide range of scenarios.

A.2 Proof that σ Defines an Upper Bound on $\hat{\mathcal{L}}^\sigma$

Let us assume that SGD optimization has reached a stationary point where the derivative w.r.t. all GMM parameters is 0. In this situation, we claim that the only way to increase the loss is by manipulating σ. We show here that $\frac{\partial \hat{\mathcal{L}}^\sigma}{\partial \sigma} < 0 \forall \sigma > 0$, and that $\frac{\partial \hat{\mathcal{L}}^\sigma}{\partial \sigma} = 0$ for $\sigma = 0$. This means that the loss can be increased by decreasing σ, up to the point where $\sigma = 0$.

For each sample, the 2D profile of $\log(\pi_k \mathcal{N}_k) \equiv f_k$ is assumed to be radially symmetric, centered on the best-matching component k^* and decreases with the distance as a function of $||k - k^*||$. We thus have $f_k = f_k(r)$ with $r \equiv ||k - k^*||$. Passing to the continuous domain, the indices in the Gaussian "smoothing filter" g_{k^*k} become continuous variables, and we have $g_{k^*k} \rightarrow g(||k - k^*||, \sigma) \equiv g(r, \sigma)$. Similarly, $f_k(r) \rightarrow f(r)$. Using 2D polar coordinates, the smoothed max-component likelihood $\hat{\mathcal{L}}^\sigma$ becomes a polar integral around the position of the best-matching component: $\hat{\mathcal{L}}^\sigma \sim \int_{\mathbb{R}^2} g(r, \sigma) f(r) dr d\phi$. We are interested in the change of $\hat{\mathcal{L}}^\sigma$ when σ undergoes an infinitesimal change. It is trivial to show that for the special case of a constant log-probability profile, i.e., $f(r) = L$, $\mathcal{L}^\sigma$ does not depend on σ because Gaussians are normalized, and that the derivative w.r.t. σ vanishes:

$$\begin{aligned}
\frac{d\hat{\mathcal{L}}^\sigma}{d\sigma} &\sim \int_0^\infty dr \Big(\frac{r^2}{\sigma^2} - 1 \Big) \exp(-\frac{r^2}{2\sigma^2}) L \\
&= L \int_0^\sigma dr \Big(\frac{r^2}{\sigma^2} - 1 \Big) \exp(-\frac{r^2}{2\sigma^2}) - L \int_\sigma^\infty \Big(\frac{r^2}{\sigma^2} - 1 \Big) \exp(-\frac{r^2}{2\sigma^2}) \\
&\equiv L\mathcal{N} - L\mathcal{P}
\end{aligned} \tag{12}$$

where we have split the integral into parts where the derivative w.r.t. σ is negative($\mathcal{N}$) and positive ($\mathcal{P}$). We know that $\mathcal{N} = \mathcal{P}$ since the derivative must be zero for a constant function $f(r) = L$ due to the fact that Gaussians are normalized to the same value regardless of σ.

For a function $f(r)$ that satisfies $f(r) > L \forall r \in [0, \sigma[$ and $f(r) < L \forall r \in]\sigma, \infty[$, the inner and outer parts of the integral behave as follows:

$$\begin{aligned} \tilde{\mathcal{N}} &= \int_0^\sigma g(r)\Big(\frac{r^2}{\sigma^2} - 1\Big) f(r) < \int_0^\sigma g(r)\Big(\frac{r^2}{\sigma^2} - 1\Big) L = L\mathcal{N} \\ \tilde{\mathcal{P}} &= \int_\sigma^\infty g(r)\Big(\frac{r^2}{\sigma^2} - 1\Big) f(r) < \int_\sigma^\infty g(r)\Big(\frac{r^2}{\sigma^2} - 1\Big) L = L\mathcal{P} \end{aligned} \tag{13}$$

since $f(r)$ is minorized/majorized by L by assumption, and the contributions in both integrals have the same sign for the whole domain of integration. Thus, it is shown that, for $\sigma > 0$

$$\frac{d\hat{\mathcal{L}}^\sigma}{d\sigma} = \tilde{\mathcal{N}} - \tilde{\mathcal{P}} < L\mathcal{N} - L\mathcal{P} = 0 \tag{14}$$

and, furthermore, that this derivative is zero for $\sigma = 0$ because $\hat{\mathcal{L}}^\sigma$ no longer depends on σ for this case.

Taking everything into consideration, in a situation where the log-likelihood $\hat{\mathcal{L}}^\sigma$ has reached a stationary point for a given value of σ, we have shown that:

- The value of $\hat{\mathcal{L}}^\sigma$ depends on σ.
- Without changing the log-probabilities, we can increase $\hat{\mathcal{L}}^\sigma$ by reducing σ, assuming that the log-probabilities are mildly decreasing around the BMU.
- Increasing $\hat{\mathcal{L}}^\sigma$ works as long as $\sigma > 0$. At $\sigma = 0$ the derivative becomes 0.

Thus, σ indeed defines an upper bound to $\hat{\mathcal{L}}^\sigma$ which can be increased by decreasing σ. The assumption of log-probabilities that decrease around the BMU is reasonable since such a profile maximizes $\hat{\mathcal{L}}^\sigma$. All functions $f(r)$ that, e.g., decrease monotonically around the BMU, fulfill this criterion, where the precise form of the decrease is irrelevant. This proof works identically when not resorting to integrals but using discrete sums.

A.3 Log-Likelihood Gradients

The gradients of $\hat{\mathcal{L}}$ read

$$\begin{aligned} \frac{\partial \hat{\mathcal{L}}}{\partial \boldsymbol{\mu}_k} &= \mathbb{E}_n \left[\boldsymbol{P}_k \left(\boldsymbol{x}_n - \boldsymbol{\mu}_k \right) \delta_{kk^*} \right] \\ \frac{\partial \hat{\mathcal{L}}}{\partial \boldsymbol{P}_k} &= \mathbb{E}_n \left[\left((\boldsymbol{P}_k)^{-1} - (\boldsymbol{x}_n - \boldsymbol{\mu}_k)(\boldsymbol{x}_n - \boldsymbol{\mu}_k)^T \right) \delta_{kk^*} \right] \\ \frac{\partial \hat{\mathcal{L}}}{\partial \pi_k} &= \pi_k^{-1} \mathbb{E}_n \left[\delta_{kk^*} \right]. \end{aligned} \tag{15}$$

The gradients of $\mathcal{L}$ are obtained by replacing δ_{kk^*} by the standard GMM responsibilities γ_{nk}. For the case of a degenerate solution when optimizing $\mathcal{L}$, only a single component k^* has a weight close to 1, with its centroid and covariance matrix are given by the mean and covariance of the data: $\pi_{k^*} \approx 1$, $\boldsymbol{\mu}_{k^*} = \mathbb{E}[\boldsymbol{X}]$, $\boldsymbol{P}_{k^*}^{-1} = \mathrm{Cov}(\boldsymbol{X})$. In this case, the gradients w.r.t $\boldsymbol{\mu}$ and $\boldsymbol{P}$ vanish. The gradient w.r.t. π_k does not vanish, but is δ_{kk^*} which vanishes after enforcing the normalization constraint.

A.4 Visualization of High-dimensional sEM Outcomes

Fig. 3 was obtained after training GMMs by sEM on both the Fruits 360 and the SVHN dataset. It should be compared to Fig. 2, where an identical procedure was used to visualize centroids of SGD-trained GMMs. It is notable that the effect of unconverged components does not occur at all for our SGD approach, which is due to the annealing mechanism that "drags" unconverged components along.

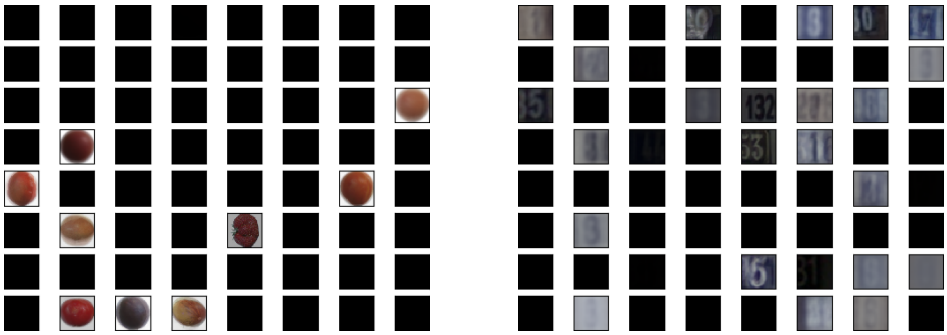

Figure 3: Visualization of centroids after exemplary training runs (3 epochs) on high-dimensional datasets for sEM: Fruits 360 (left, 30 000 dimensions) and SVHN (right, 3 000 dimensions). Component entries are displayed "as is", meaning that low brightness means low RGB values. Visibly, many GMM components remain unconverged, which is analogous to a sparse-component solution and explains the low log-likelihood values especially for these high-dimensional datasets.

A.5 Visualization of 2D Annealing Grid

In Figure 4, three different states of the $\boldsymbol{g}_k$ are visualized, depending on $\sigma(t)$. Darker pixels indicate larger values. Each $\boldsymbol{g}_k$ is assigned to a single GMM component k, which is why the $\boldsymbol{g}_k$ are arranged on the same $\sqrt{K} \times \sqrt{K}$ grid we place the components themselves. An intuitive interpretation of a particular $\boldsymbol{g}_k$ is that it encodes the contribution of neighbouring component log-probabilities on the log-probability of component k entering into max-computation. Over time, $\sigma(t)$ is reduced (middle and right pictures) and thus only component k contributes. Please note that the grid we place the components on is periodic for simplicity, so the $\boldsymbol{g}_k$ are themselves periodic.

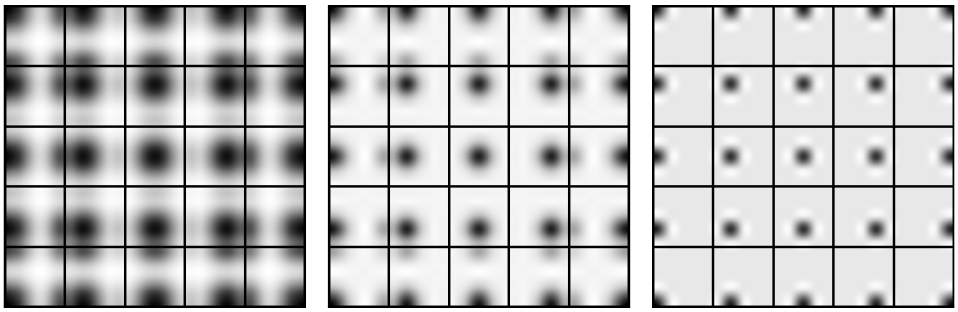

Figure 4: Visualization of different centered Gaussian function $\boldsymbol{g}_k$ states controlled by σ.

A.6 DIAGRAMS OF CLUSTERING COMPARISON

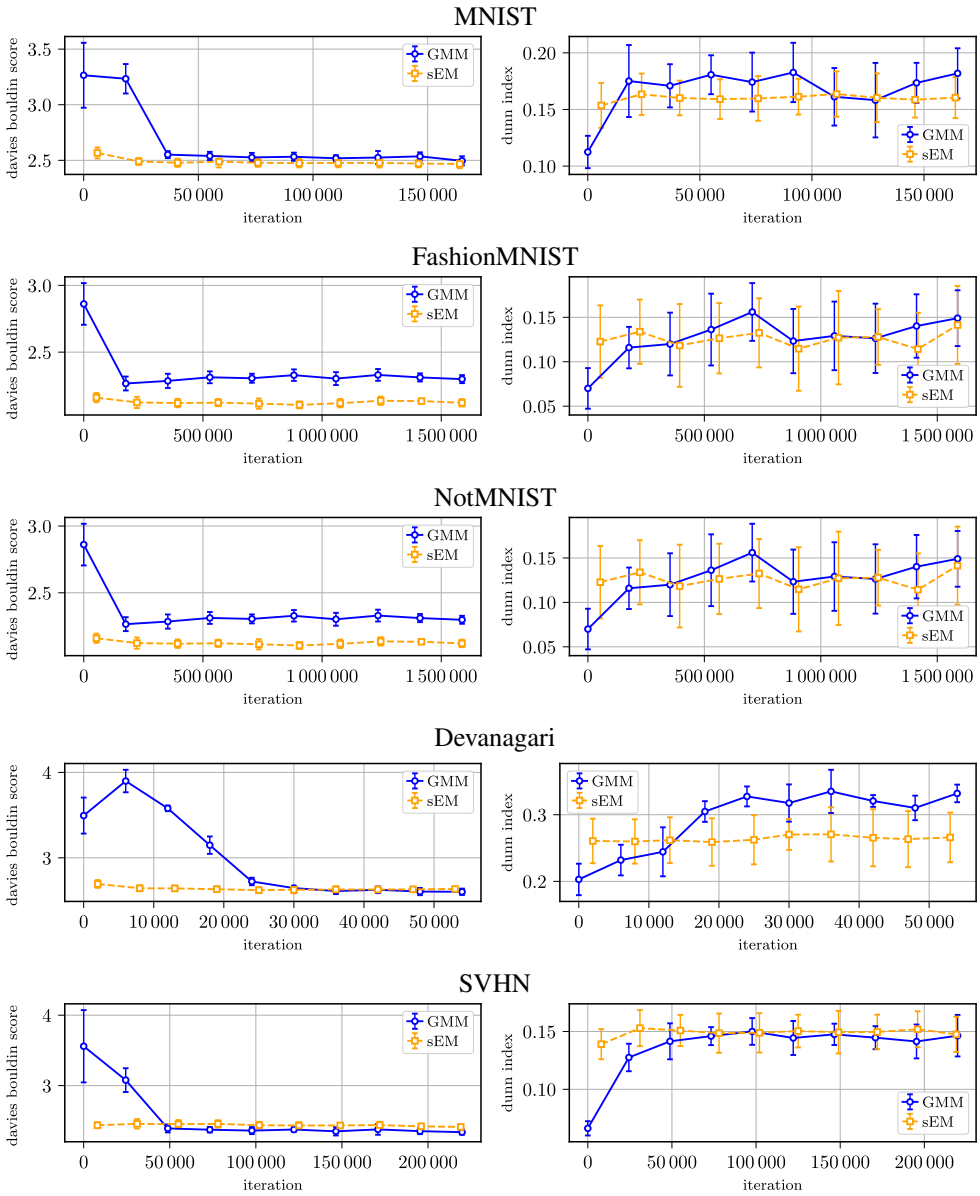

Figure 5: Trend of clustering capabilities for sEM and SGD trained GMM. Comparison by Davies-Bouldin score (smaller is better) and Dunn index (higher is better) for the datasets MNIST, FashionMNIST, NotMNIST, Devanagari and SVHN. The lines visualize the average metric score/index values of 10 repetitions with its standard deviation.

A.7 Diagrams of Concept Drift Experiments

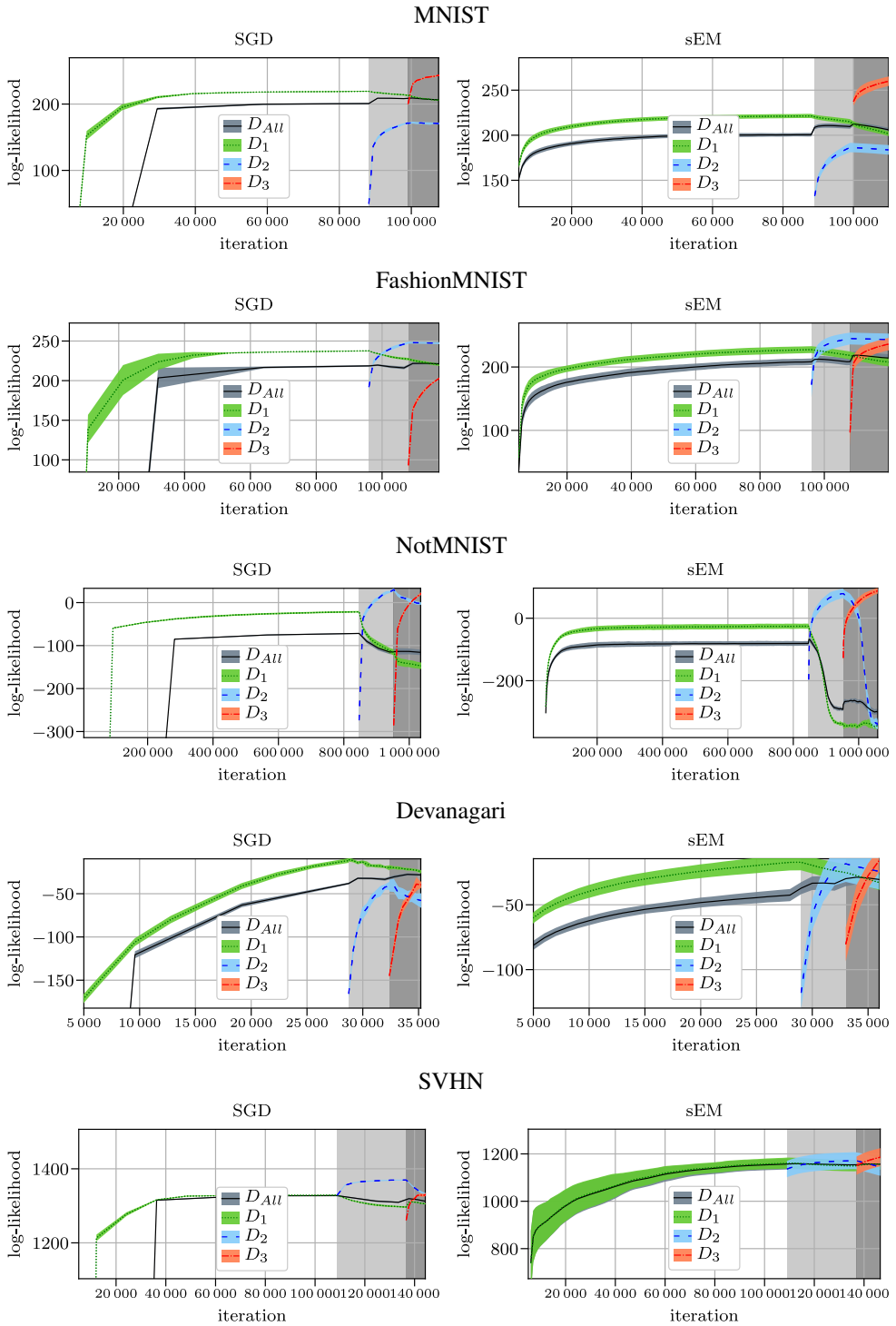

Figure 6: Temporal trend of losses during GMM training for the datasets MNIST, FashionMNIST, NotMNIST, Devanagari and SVHN and corresponding slice variants. Each experiment for SGD and sEM training are performed 10 times. The different lines visualize the average log-likelihood values depending on the task (background color), while the surfaces show the standard deviation.